Available online at www.sciencedirect.com
ScienceDirect
Journal of Photochemistry and Photobiology A: Chemistry 186 (2007) 57–64
Journal of Photochemistry and Photobiology A:Chemistry
www.elsevier.com/locate/jphotochem

Preferential noncovalent immunoglobulin G adsorption onto hydrophobic segments of multi-functional metallic nanowires

Amanda M. Fond [a], Nira S. Birenbaum [a], Edward J. Felton [b], Daniel H. Reich [b], Gerald J. Meyer [a,*]

[a] *Departments of Chemistry and Materials Science and Engineering, Johns Hopkins University, Baltimore, MD 21218, United States*
[b] *Department of Physics and Astronomy, Johns Hopkins University, Baltimore, MD 21218, United States*

Received 9 June 2006; received in revised form 11 July 2006; accepted 12 July 2006
Available online 25 July 2006

Abstract

Two-segment metallic nanowires fabricated by templated electrodeposition were functionalized with immunoglobulin G (IgG). The functionalization was selective with protein adsorption occurring preferentially on the nickel or gold segment of the wire. This selectivity was achieved by utilizing recent advances in self-assembly of organic ligands at planar electrodes. Two-component Ni–Au nanowires were functionalized to yield both a hydrophilic segment and a hydrophobic segment. Comparative studies with single segment gold and nickel nanowires were also performed. The functionalization procedures allowed the hydrophilic and hydrophobic groups to be directed to either the gold or nickel portion. The protein resistant properties of these bifunctional nanowires were studied and quantified by optical and fluorescence microscopies. A weak non-specific adsorption of IgG to hydrophilic nanowires or nanowire segments was observed. IgG bound strongly to hydrophobic nanowires or nanowire segments. Isotherms were well described by the Langmuir model from which limiting surface coverages near that expected for a monolayer ($(6.0 \pm 0.5) \times 10^{-11}$ mol/cm^2) and an equilibrium constant of $K = (3 \pm 2) \times 10^6$ M^{-1} were abstracted. Contact angle measurements on planar Au and Ni surfaces correlated well with the degree of protein adsorption to nanowires.

Keywords: Protein adsorption; Immunoglobulin G; Nanowires

1. Introduction

The adsorption of proteins to nanoparticle surfaces is an important research area. As nanotechnology becomes more integrated into other fields of science, nanoparticles are emerging as essential components in drug delivery and gene therapy systems [1]. The ability to control passive protein adsorption is a critical element in this research. On planar surfaces, self-assembled monolayers (SAMs) have been used to tune the degree of protein adsorption to different surfaces of varying hydrophilicity. Prime and Whitesides showed that SAMs on planar gold composed of a mixture of hydrophobic and hydrophilic compounds were more resistant to protein adsorption as the fraction of hydrophilic molecules in the monolayer increased [2]. They also demonstrated that monolayers terminated in oligo(ethylene glycol) groups were the most effective at preventing the non-covalent attachment of a variety of proteins.

In this manuscript, we reveal that protein resistance can be achieved on several non-planar metallic surfaces by utilizing the specific binding of ligand headgroups to surfaces. In particular, we demonstrate the selective adsorption of IgG to discrete segments of bifunctional metallic nanowires as illustrated in Fig. 1. These high-aspect ratio nanoparticles are composed of different metal components in distinct segments, allowing for spatial separation of functional groups [3,4]. Two types of functionalized nanowire surfaces were used in this study: methyl-terminated monolayers (abbreviated as Ni|CH_3 or Au|CH_3 on nickel or gold surfaces, respectively), and ethylene glycol-terminated monolayers (abbreviated as Ni|EG_n or Au|EG_6).

2. Experimental

2.1. Materials

Nickel(II) chloride ($NiCl_2 \cdot 6H_2O$) and nickel sulfamate ($Ni(H_2NSO_3)_2 \cdot 4H_2O$) 50% (w/w) aqueous solution were procured from Alfa Aesar. 434 HS, a gold electrodeposition

* Corresponding author. Tel.: +1 410 516 7319.
E-mail address: meyer@jhu.edu (G.J. Meyer).

1010-6030/$ – see front matter © 2006 Elsevier B.V. All rights reserved.
doi:10.1016/j.jphotochem.2006.07.011

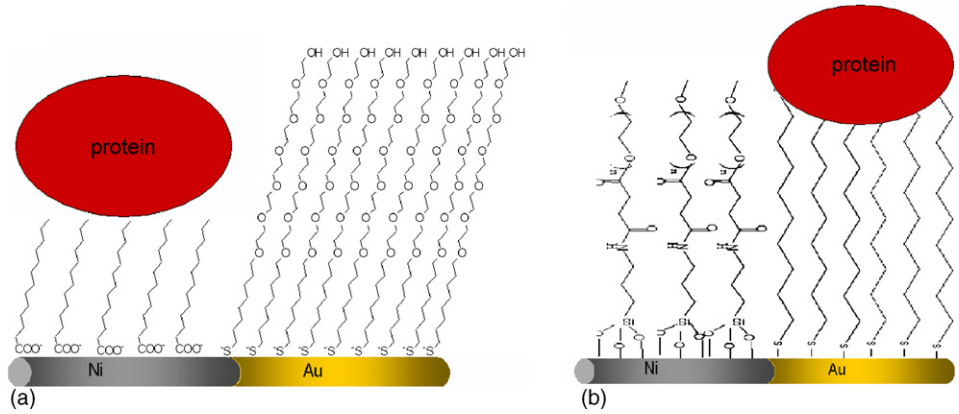

Fig. 1. Types of nickel–gold nanowires prepared in this work: (a) nickel segment functionalized with palmitic acid and gold segment functionalized with (1-mercaptoundec-11-yl)-hexaethylene glycol. The segments are abbreviated, Ni|CH_3 and Au|EG_6, respectively. (b) Nickel segment functionalized with poly(oxy-1,2ethanediyl),α-(1,methoxy)-ω-[1,4-dioxo-4-[[3-triethoxysilyl)propyl]amino]butoxy] and gold segment functionalized with nonylmercaptan, abbreviated Ni|EG_n and Au|CH_3, respectively. Superimposed on the idealized nanowires is the expected location of protein adsorption.

solution containing 0.25 troy ounce gold per quart, was purchased from Technic, Inc. Hexa(ethylene glycol), 1-bromo-11-undecene, acetic acid thiol, nonylmercaptan and palmitic acid were purchased from Aldrich. Horse heart myoglobin and methoxypolyethylene glycol succinate *N*-hydroxysuccinimide ester (50%, molecular weight ~5000) were obtained from Sigma. Alexa Fluor® 594 goat anti-mouse IgG and Alexa Fluor® 555 goat anti-rabbit IgG (H + L) were purchased from Molecular Probes, Inc. 3-Aminopropyltriethoxysilane was purchased from Strem Chemicals. Sodium bicarbonate was purchased from EM Science and boric acid was purchased from Fisher. All compounds were used as received.

2.2. Nanowire fabrication

The nanowires were fabricated by templated electrodeposition into nanoporous alumina membranes, as has been previously described [5]. Using membranes with a nominal pore diameter of 0.1 μm, 10–25 μm long gold, nickel, and two-part nickel–gold nanowires were synthesized and isolated by standard procedures [6]. Analysis by scanning electron microscopy (JEOL 6700F) revealed idealized cylindrical nanowire geometry. Nickel was deposited from an aqueous solution of 20 g/L $NiCl_2{\cdot}6H_2O$, 15 g/L $Ni(H_2NSO_3)_2{\cdot}4H_2O$ and 20 g/L H_3BO_3 at −1.0 V versus Ag/AgCl. Gold was deposited at −0.7 V versus Ag/AgCl from a commercial deposition (434 HS) solution containing potassium aurocyanate and potassium oxalate. Two-part nanowires were synthesized by first depositing gold, replacing the deposition solution, and then depositing nickel.

2.3. Synthesis of (1-mercaptoundec-11-yl)-hexaethylene glycol

$HS(CH_2)_{11}(OCH_2CH_2)_6OH$, ($EG_6$-SH), was synthesized in three steps with a modified literature preparation [7]. The synthesis is outlined in Scheme 1.

2.3.1. Step 1: preparation of undec-1-en-11-ylhexa(ethylene glycol)

25 g of hexa(ethylene glycol) (88.5 mmol) was heated at 100 °C with 700 μL of 50% NaOH (8.8 mmol) for 30 min

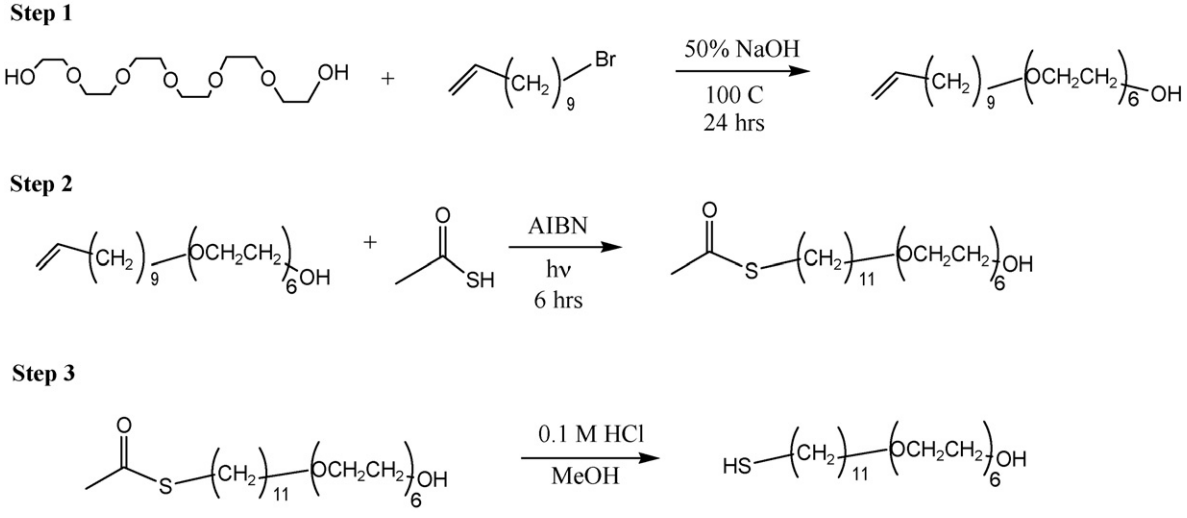

Scheme 1. Synthesis of (1-mercaptoundec-11-yl)-hexaethylene glycol.

in an argon-filled flask. To that, 2 g of 1-bromo-11-undecene (8.6 mmol) was then added. The reaction was stirred for 24 h and allowed to cool. The mixture was diluted with ∼15 mL deionized water, extracted with 250 mL hexane, dried over $MgSO_4$, and filtered. The solvent was removed *in vacuo* to give 2.77 g of a dark yellow oil. This product was flushed through a short plug of silica gel with CH_2Cl_2. Evaporation of the solvent gave 1.88 g of purified product. ^{1}H NMR δ (300 MHz, $CDCl_3$): 1.24 (br, s, 12H), 1.53 (qui, 2H), 2.01 (q, 2H), 2.73 (br, s, 1H), 3.40 (t, 2H), 3.54–3.69 (m, 24H), 4.91(m, 2H), 5.76 (m, 1H).

2.3.2. Step 2: preparation of [1-[(methylcarbonyl) thio]undec-11-yl]hexa(ethylene glycol)

1.3 g of CH_2=$CH(CH_2)_9(OCH_2CH_2)_6OH$ (3 mmol) and 760 mg of acetic acid thiol (10 mmol) were dissolved in 10 mL methanol which had been distilled from K_2CO_3. This solution was degassed by three successive freeze-pump-thaw cycles. Approximately 5–10 mg of AIBN was added, and the reaction flask was sealed under argon. The reaction mixture was irradiated for 7 h at room temperature with a 450 W mercury lamp. A flocculent white solid was removed by filtration and the remaining yellow solution was concentrated *in vacuo*, giving 1.46 g of a yellow oil. The product was purified by column chromatography on silica gel, using CH_2Cl_2 and then 2% MeOH in CH_2Cl_2 as the eluents. ^{1}H NMR δ (300 MHz, $CDCl_3$): 1.2 (br, s, 14H), 1.52 (m, 4H), 2.28 (s, 3H), 2.69 (br, s, 1H), 2.81 (t, 2H), 3.40 (t, 2H) 3.54–3.69 (m, 24H).

2.3.3. Step 3: preparation of (1-mercaptoundec-11-yl)-hexaethylene glycol

500 mg of $CH_3OS(CH_2)_{11}(OCH_2CH_2)_6OH$ were dissolved in 10 mL MeOH and 125 μL of HCl were added. In order to prevent oxidation to the disulfide, the solution was purged with argon. After 4 h of refluxing, the pH was adjusted to 7 by the dropwise addition of 5% NaOH. This solution was then extracted with CH_2Cl_2, dried over $MgSO_4$, and filtered. Evaporation of the solvent gave 300 mg of the pure product as a dark yellow oil. ^{1}H NMR δ (300 MHz, $CDCl_3$): 1.25 (br, s, 14H), 1.34 (t, 1H), 1.54 (m, 4H), 2.52 (q, 2H) 2.64 (br, s, 1H), 3.53 (t, 2H), 3.54–3.69 (m, 24H).

2.4. Planar surface functionalization

Planar metallic films were deposited on glass microscope slides (Fisher). Glass slides were cleaned in sulfuric acid with Nochromix (an oxidizing agent), rinsed in deionized water, and dried under nitrogen. Planar nickel and gold films were deposited in a thermal evaporator. Nickel was deposited (50 Å) directly onto glass; gold films (50 Å) were deposited on top of an adhesion layer of chromium (25 Å).

Hydrophobic planar surfaces were achieved by soaking nickel or gold evaporated films overnight in a 1 mM ethanolic palmitic acid or 1 mM ethanolic nonylmercaptan solution, respectively. Likewise, hydrophilic planar gold surfaces were created by immersing a gold film in a 1 mM ethanolic EG_6-SH solution. Hydrophilic planar nickel surfaces were produced by equilibrating an evaporated nickel film in a 1 mM ethanolic 3-aminopropyltriethoxysilane solution for 24 h. The film was then rinsed with ethanol and then 0.1 M sodium bicarbonate (pH 8.3) buffer and put into 0.1 mg/mL methoxypolyethylene glycol succinate *N*-hydroxysuccinimide ester in buffer solution and left to react for 1 h.

2.5. Contact angle goniometry

Water contact angle measurements were determined at ambient temperatures in air with a NRL CA goniometer (Model No.: 100-00-15) from Rame'-Hart, Inc. A 50 μL droplet of deionized water was pipetted onto the planar substrate, and measurements were obtained using the sessile-drop method [8]. The contact angles reported are an average of at least five measurements taken at different locations on the surface.

2.6. Nanowire functionalization

To create hydrophobic, alkyl-terminated nickel surfaces, a batch of nickel wires were combined with a 1 mM ethanolic solution of palmitic acid, $C_{15}H_{31}CO_2H$, overnight. The nanowires were cleaned using successive washes with ethanol. The wires were collected either magnetically or by centrifugation and the supernatant was decanted off. Neat solvent was added and the nanowires were redispersed by ultrasonication. This process was repeated several times. To create hydrophilic, protein-resistant gold surfaces, gold nanowires were placed in a 1 mM ethanolic solution of EG_6-SH overnight. Bimetallic nanowires with both a nickel and gold component were functionalized in one step, by adding the wires to a solution containing both EG_6-SH and palmitic acid [9].

The inverse functionalization was also achieved. Gold wires were added to a 1 mM ethanolic solution of nonylmercaptan overnight to attain hydrophobicity. A hydrophilic nickel segment was created by a two-step process. The wires were placed in a 1 mM ethanolic 3-aminopropyltriethoxysilane solution overnight and successively washed with ethanol and 0.1 M sodium bicarbonate (pH 8.3) buffer. To the wire suspension, 0.1 mg/mL of methoxypolyethylene glycol succinate *N*-hydroxysuccinimide ester was added and sonicated intermittently for 1 h [10].

2.7. Protein adsorption

2.7.1. Single-component wires

Ni|CH_3 and Au|EG_6 nanowires were rinsed with ethanol and water, and immersed in an aqueous solution of Alexa Fluor® 594 goat anti-mouse IgG, a fluorescently-tagged antibody. The protein was added to a 1 mL suspension of nanowires in phosphate buffered saline (PBS) to a final concentration of 20 μg/mL. The nanowires were exposed to the protein solution for time periods ranging from 1 min to 1 h, with intermittent sonication. The wires were then magnetically collected, rinsed with water, and spin-coated onto glass coverslips to be observed under a fluorescence microscope.

2.7.2. Multi-component wires

Bifunctional Ni|CH_3–Au|EG_6 and Ni|EG_n–Au|CH_3 wires and unfunctionalized Ni–Au wires were subsequently rinsed with ethanol, water, and PBS, respectively. Alexa Fluor® 555 goat anti-rabbit IgG (H + L) was added to the nanowire suspension at a concentration of 10 μg/mL. The wires were exposed to the protein for 20 min. They were then collected with a magnet, washed with PBS and water, respectively, and spun-out onto a glass coverslip at 1200 rpm for 1 min.

2.8. Optical microscopy

Fluorescence and reflection microscopy images were collected with a Nikon Eclipse TE200 inverted microscope equipped with a Hamamatsu Orca CCD camera. MetaVue imaging software was used for the data collection and manipulation. The excitation light source was a 100 W mercury arc lamp (Ushio, Japan) that was attenuated using neutral density filters. Nanowire reflectivity was observed with the aid of a 50/50 mirror and a 600–650 nm band pass filter. Alexa Fluor® 594 and 555 fluorophores were visualized using the G-2E/C filter cube (Nikon), which provides excitation from 525 to 555 nm, and allows emission from 590 to 650 nm. For fluorescence images, a 2 s exposure time was used, while the exposure time was set to 0.42 ms with the addition of a neutral density filter (ND8) for reflection images. To measure nanowire pixel intensities, each reflection image was thresholded and a region of interest was drawn around the nanowire. This region was transferred to the corresponding fluorescence image, and the average pixel intensity within the region was calculated. To account for exceptionally bright spots of fluorescence from aggregated or precipitated proteins, 5–8% of the brightest pixels were eliminated from the average. The average intensity of the background was subtracted from this value to give the average fluorescence intensities of the nanowires.

2.9. Quantification of protein adsorption

Isotherms for protein adsorption to hydrophobic nanowire surfaces were quantified at room temperature. These experiments employed horse heart myoglobin as the adsorbate instead of the Alexa Fluor® conjugate, since the strong molar absorptivity of the native heme allowed for facile determination of small myoglobin concentrations in solution. Aqueous solutions of myoglobin ranging in concentration from 0.3 to 5 μM were combined with 0.5 mg of 5 μm long Ni|CH_3 nanowires, and mixed for 20 min. The nanowires, which have a total surface area of ~7.5 cm^2, were delivered as an aqueous suspension with less than 1% ethanol added to help solvate the wires. Blank samples containing equivalent myoglobin concentrations but excluding the wires were made following the same protocol and placed in the mixer. After mixing, the absorbance at 408 nm was measured for each sample. The concentration difference between the samples with wires and those without was calculated from the reported extinction coefficient of myoglobin, $E_{408\ nm} = 179{,}000\ M^{-1}\ cm^{-1}$ [11]. This change in concentration was then used to determine the surface coverage of myoglobin on the Ni|CH_3 nanowires.

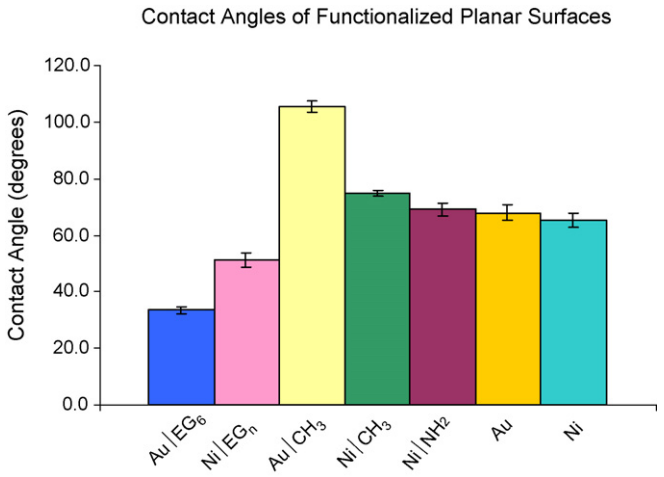

Fig. 2. Contact angle measurements of planar surfaces functionalized with various organic monolayers.

3. Results

3.1. Contact angle goniometry

Contact angle measurements were obtained to characterize planar surfaces with specific organic monolayers before apply-

Table 1
Contact angles measured in this work and literature values

Substrate	Organic layer	Contact angle	Reference
Ni	None	65 ± 2	This work
	Palmitic Acid	75 ± 1	This work
	3-Aminopropyltrimethoxysilane	69 ± 2	This work
	3-Aminopropyltrimethoxysilane-(EG)n	51 ± 2	This work
Au	None	68 ± 3; 74	This work; 12(a)
	Nonylmercaptan	105 ± 2	This work
	Octylmercaptan	108	12(b)
	(1-Mercaptoundec-11-yl)-hexaethylene glycol	34 ± 1; 38[a]; 25[b]	This work; 12(c)
Si/SiO_2	*n*-Octadecyltrimethoxysilane	105	12(d)
	3-Aminopropyldimethylethoxysilane	60	12(e)

[a] Represents an advancing contact angle measurement.
[b] Represents a receding contact angle measurement.

ing the same functionalization techniques to nanowires. The contact angles reported in Fig. 2 were consistent with previously published data as shown in Table 1 [12]. In addition, wettability of the films coincided with the desired hydrophobicity.

The surfaces functionalized with highly ordered hydrophobic monolayers ($Au|CH_3$), yielded large contact angles, while methyl-functionalized nickel surfaces ($Ni|CH_3$) proved to only be moderately wettable. This observation can be explained by the structural stability of alkanethiolate monolayers on gold [13] and the presence of monolayer defects due to the presence of a native oxide layer on nickel [14]. In addition, planar surfaces with amine terminal groups ($Ni|NH_2$) and no functionalization (Ni and Au) showed moderate wettability. However, when an ethylene glycol moiety was coupled to the amine-terminated surface ($Ni|EG_n$), the wettability of the surface increased, indicating a decrease in hydrophobicity. Ethylene glycol functionalized gold surfaces ($Au|EG_6$) also proved to be especially hydrophilic.

3.2. Protein adsorption to single-component nanowires

$Ni|CH_3$ nanowires were exposed to fluorescent-tagged IgG protein for varying lengths of time in order to find the minimum amount of time needed to achieve irreversible passive adsorption of the protein to the hydrophobic nanowire surface. Nanowires were placed in the protein solution for periods of 1, 5, 15, 30 or 60 min and sonicated intermittently. Reaction times longer than 15 min yielded the same protein surface coverages. Therefore, 20 min was chosen as a convenient reaction time for all subsequent protein adsorption experiments.

Functionalized single component nickel and gold wires were combined with fluorescent-tagged IgG to compare the degree of protein adsorption on hydrophobic and hydrophilic nanowire surfaces, respectively. In general, methyl-terminated nickel nanowires showed bright fluorescence while ethylene glycol-terminated gold nanowires were very dim or completely non-fluorescent (Fig. 3).

3.3. Protein adsorption isotherms

The adsorption of myoglobin to $Ni|CH_3$ nanowires exhibited a Langmuir-type concentration dependence [15]. According to this model, the surface coverage Γ of an adsorbate rises with the equilibrium solution concentration until the substrate is sat-

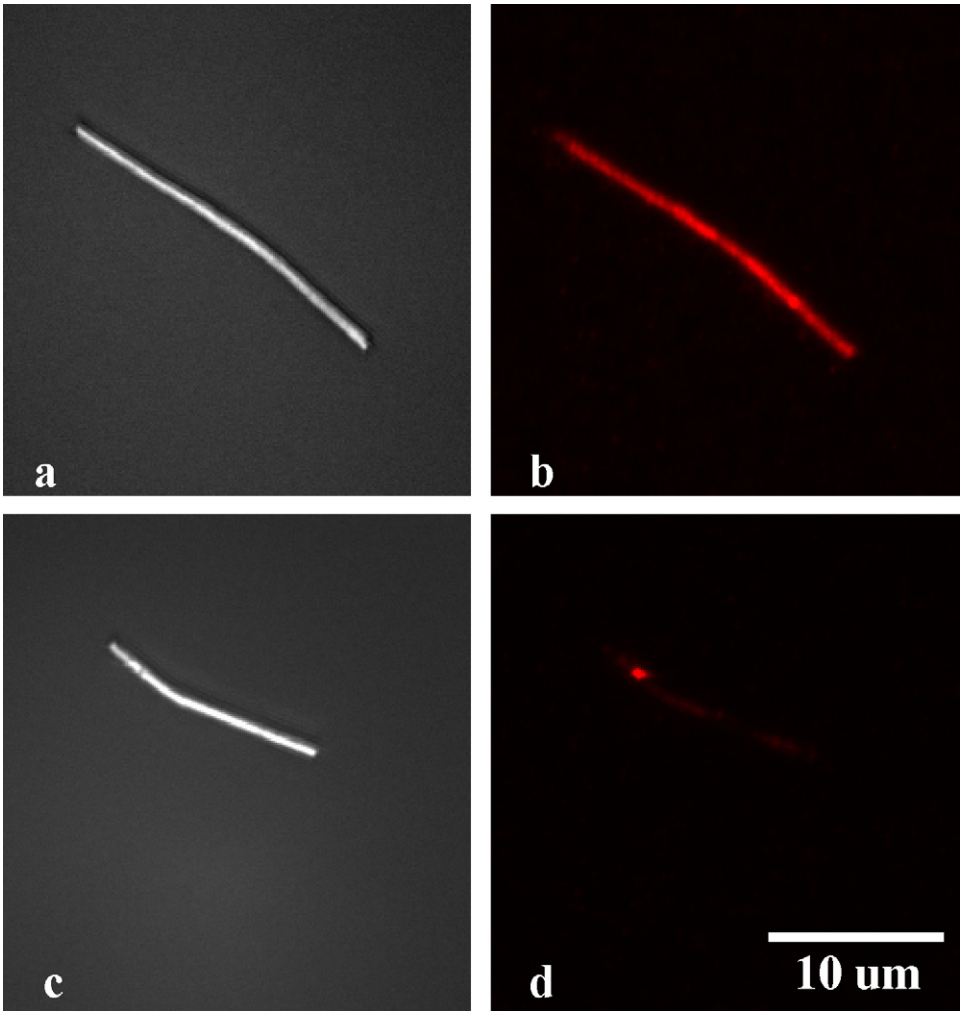

Fig. 3. Goat anti-mouse IgG protein adsorption to single component nanowires. (a) Reflection image of $Ni|CH_3$ nanowire after reaction with fluorescent protein. (b) Fluorescence image of same nanowire in (a). (c) Reflection image of $Au|EG_6$ nanowire after reaction with this fluorescent protein. (d) Fluorescence image of same nanowire in (c).

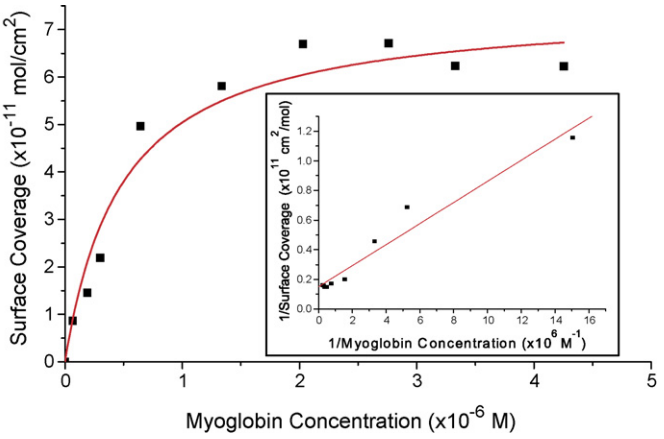

Fig. 4. Adsorption isotherm for myoglobin on hydrophobic nickel nanowires. For a large number of samples a saturation surface coverage of $(6.0 \pm 0.5) \times 10^{-11}$ mol/cm^2 was measured. The inset shows a double-reciprocal plot of this data from which an equilibrium constant of $K = (3 \pm 2) \times 10^6$ M^{-1} was abstracted.

urated. The model is described mathematically by the equation:

$$\Gamma = \Gamma_{\max} \frac{K_A\,[\mathrm{Mb}]}{1 + K_A\,[\mathrm{Mb}]} \quad (1)$$

where $\Gamma_{\max}$ is the saturation surface coverage and K_A is the equilibrium constant for protein adsorption. Fig. 4 shows a plot of myoglobin surface coverage versus concentration. Visual inspection of this data indicated that the surface coverage becomes saturated when the solution concentration was greater than approximately 2 μM. A saturation surface coverage of $\Gamma_{\max}$ was determined to be $(6.0 \pm 0.5) \times 10^{-11}$ mol/cm^2. The inset in Fig. 4 shows a double-reciprocal plot of the data from which an equilibrium constant was abstracted, $K = (3 \pm 2) \times 10^6$ M^{-1}.

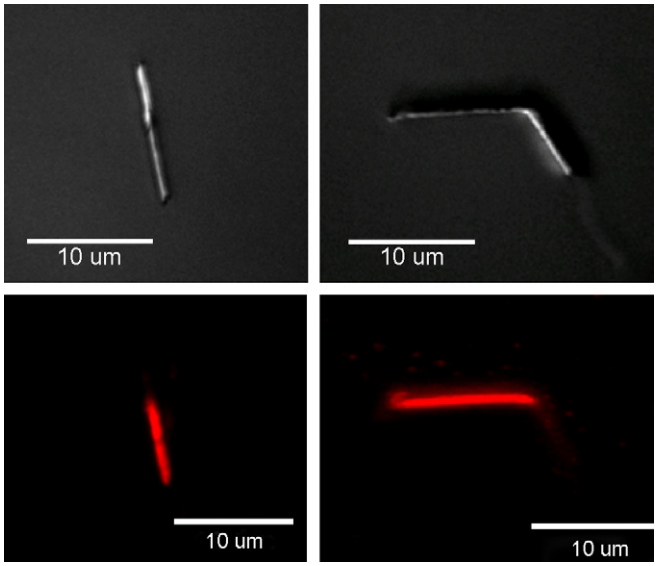

Fig. 5. Selective adsorption of goat anti-rabbit IgG protein to bifunctional nanowires. Upper row: reflection images of two Ni|CH_3–Au|EG_6 nanowires which have been combined with fluorescent protein. The darker segment is nickel and the brighter segment is gold. Bottom row: corresponding fluorescence images, showing protein adsorption localized on the nickel segment.

3.4. Protein adsorption to multi-segment nanowires

When bifunctional Ni|CH_3–Au|EG_6 nanowires were combined with a fluorescent antibody, selective adsorption of the protein to the hydrophobic nickel segment was observed. Several representative images are shown in Fig. 5. In the upper row, reflection images show the two distinct nanowire segments, where gold is the shiny section and nickel is the more dull sec-

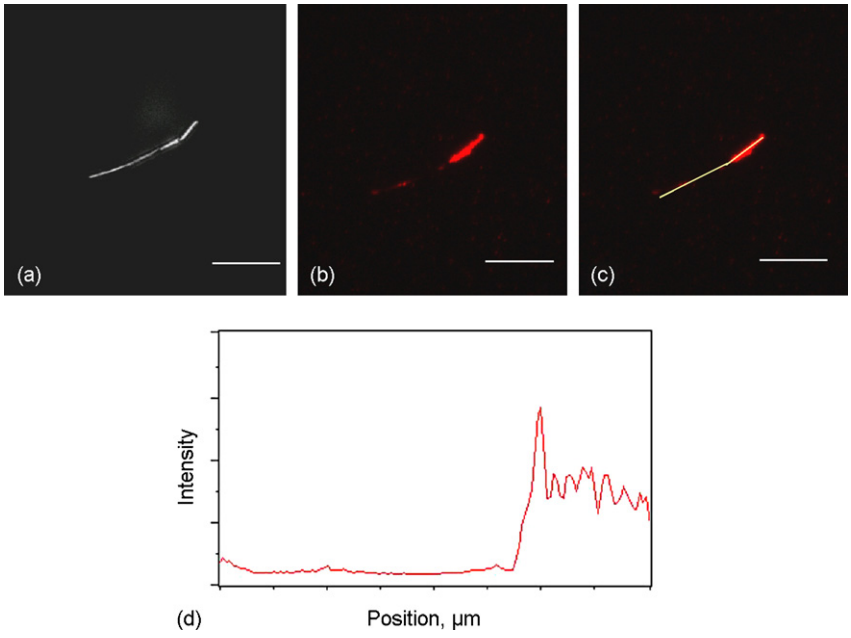

Fig. 6. Selective goat anti-rabbit IgG protein absorption to bifunctional Ni|EG_n–Au|CH_3 exposed to fluorescent protein. (a) Reflection image of the nanowire. The brighter of the two segments represents the gold segment of the nanowire. (b) The corresponding fluorescent image that demonstrates selective protein absorption to the hydrophobic gold segment. (c) An overlay of the fluorescent and reflection images. (d) A line scan analysis of the fluorescence intensity along the length of the nanowire. The scale bar represents 10 μm.

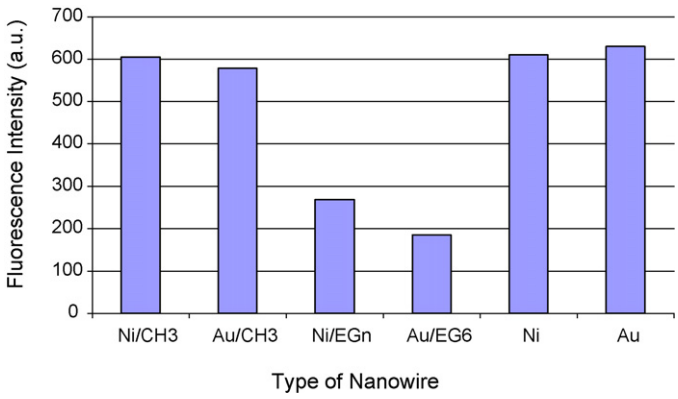

Fig. 7. Fluorescence intensity of different types of nanowires after exposure to fluorescent goat anti-rabbit IgG protein.

tion. The bottom row contains the corresponding fluorescence images of the same nanowires. In each set of images, it is clear that only the nickel portion of the nanowire is fluorescent, indicating the presence of IgG protein on only the hydrophobic segment.

Bifunctional Ni|EG_n–Au|CH_3 wires exhibited similar behavior; IgG protein was preferentially adsorbed onto the hydrophobic gold segment. Fig. 6 shows some examples of this behavior. Reflection images, the top row, differentiate the two segments of the nanowire. The corresponding fluorescent images demonstrate the preferential binding of fluorescent protein to the gold portion of the wire.

Since there appeared to be a significant distribution of fluorescence intensities for both the methyl- and ethylene glycol-terminated wires, a quantitative analysis was carried out. The fluorescence intensity of two-part Ni–Au, Ni|CH_3–Au|EG_6, and Ni|EG_n–Au|CH_3 wires were measured along the length of the wire as shown in Fig. 6. Fig. 7 shows a comparison of the average intensity values of ∼15 wire samples for different populations of nanowires.

4. Discussion

A correlation between protein adsorption to nanowires and the contact angle measured on similarly functionalized planar surfaces was discovered. Low contact angle surfaces (<60°) gave very little protein adsorption while high contact angle surfaces (>60°) gave a more uniform protein layer. The contact angle measurements performed in parallel to nanowire studies, verified the surface wettability and confirmed the expectation of an increased hydrophilic nature for surfaces terminated with ethylene glycol compared to alkyl-functionalization.

As seen in Figs. 5 and 6, single component Au|EG_6 and Ni|EG_n wires displayed a small amount of adsorbed IgG in fluorescence microscopy images. In contrast, previous studies of protein adsorption on patterned planar surfaces reported no measurable fluorescence from the EG-terminated regions [16]. A quantitative analysis showed that fluorescent-tagged IgG emission on methyl-terminated nickel and gold wires was on average three times brighter than on the ethylene glycol-terminated counterparts. This is consistent with the empirical observation from the complementary reflection and fluorescent images (Figs. 5 and 6) that protein did not adhere to the ethylene glycol-terminated nanowires.

In control experiments, IgG adsorption to unfunctionalized gold and nickel wires was examined. Fluorescence on unfunctionalized gold wires was three times more intense than on EG_6-functionalized wires, consistent with passive protein adsorption to gold. Similar behavior was observed with Ni. Thus, it is clear that the more pronounced protein resistance can be attributed to the hydrophilic EG_6-terminated surface and is not a property of the nanowire itself.

Two-part nickel–gold nanowires with a hydrophobic functionality on one segment and a hydrophilic functionality on the other were selectively resistant to IgG adsorption. The different surface chemistries of the metallic segments enable two functional groups to be spatially segregated on different regions of the nanowire [3]. In Fig. 5, several bifunctional Ni|CH_3–Au|EG_6 nanowires are shown. From these images, it is evident that the hydrophobic portion of the nanowire fluoresced more intensely, consistent with preferential IgG adsorption to the nickel segment. The same was true for Ni|EG_n–Au|CH_3. Fluorescence was observed mainly on the gold portion of the wire, further confirming the adsorption of IgG on hydrophobic surfaces and the inhibition of protein adsorption on hydrophilic surfaces.

Our results demonstrate that multi-component nanostructures can be modified at the molecular level to yield materials that spatially separate proteins in specific regions. This selectivity establishes the utility of EG-functionalization in preventing passive protein adsorption on both planar and nanowire surfaces. By analogy to studies of similar SAMs on planar surfaces [16–20], and because there is a strong precedent for the broad application of poly(ethylene glycol) coatings in protein-resistant materials [21], we believe that this result is general and can be extended to other proteins and biomolecules, as well as to application with living cells [22]. Although there has been much research involving the use of EG-terminated monolayers to pattern proteins on planar substrates, this characteristic has only recently been applied to spherical nanoparticles [21b]. The localization of two functionalities on different regions of the nanowire cannot be easily mimicked with spherical nanoparticles, and is the key feature that leads to the selective adsorption of the protein. The oxygen storage protein myoglobin was used to quantify adsorption on methyl-terminated nickel nanowires. The intense Soret absorption of the heme center enables one to quantify the amount of protein absorbed. Absorption isotherms were well described by the Langmuir model [13]. The myoglobin crystal structure indicates that the dimensions of this protein in the solid state are 44 Å × 25 Å × 44 Å, giving it a footprint of at least 11 nm^2 [23]. Thus, a monolayer of adsorbed myoglobin would be expected to give a surface coverage of 2×10^{-11} mol/cm^2, which is consistent with experimental studies [24,25]. The value measured here of Γ_{max}, $(6.0 \pm 0.5) \times 10^{-11}$ mol/cm^2 represents approximately three times more protein than that expected for a monolayer. However, the factor of three agreement is within reasonable experimental error given the idealized cylinder nanowire geometry used in the calculations and the unknown surface roughness.

In this paper, we have demonstrated that proteins adsorb to hydrophobic nanowires with high surface coverages. More specifically, we have shown that IgG adsorption to Ni–Au nanowires can be directed to occur preferentially on the nickel or the gold end by utilizing the appropriate surface functionalization. In addition, the ability to restrict protein adsorption to a defined section of a nanowire has been established. Nanoparticles with distinct regions of adsorbed protein may demonstrate novel interactions with cells, such as resistance to internalization. These properties may, in turn, prove to have useful applications in studying cell–cell interactions or the effects of mechanical and electrical forces on individual cells.

Acknowledgements

The authors acknowledge equipment support from the NSF MRSEC Grant number DMR 05-20491. The authors acknowledge support from DARPA/AFOSR Grant F49620-02-1-0307 and from The David and Lucille Packard Foundation Grant #2001-17715.

References

[1] J. Kreuter, Nanoparticles as Drug Delivery Systems, in: H.S. Nalwa (Ed.), Enclyclopedia of Nanoscience and Nanotechnology, vol. 7, American Scientific Publishers, Stevenson Ranch, CA, 2004, pp. 161–180.
[2] K.L. Prime, G.M. Whitesides, Science 252 (1991) 1164–1167.
[3] N.S. Birenbaum, B.T. Lai, C.S. Chen, D.H. Reich, G.J. Meyer, Langmuir 19 (2003) 9580–9582.
[4] (a) B.R. Martin, D.J. Dermody, B.D. Reiss, M. Fang, A. Lyon, M.J. Natan, T.E. Mallouk, Adv. Mater. 11 (1999) 1021–1025;
(b) L.A. Bauer, G.J. Meyer, D.H. Reich, Langmuir 19 (2003) 7043–7048.
[5] T.M. Whitney, J.S. Jiang, P.C. Searson, C.L. Chien, Science 261 (1993) 1316–1319.
[6] L.A. Bauer, D.H. Reich, G.J. Meyer, Langmuir 19 (2003) 7043–7048.
[7] C. Pale-Grosdemange, E.S. Simon, K.L. Prime, G.M. Whitesides, J. Am. Chem. Soc. 113 (1991) 12–20.
[8] H. Burnett, T. Shedd, G. Nellis, C. Van Peski, J. Vac. Sci. Technol. B 23 (6) (2005) 2721–2727.
[9] P.E. Laibinis, J.J. Hickman, M.S. Wrighton, G.M. Whitesides, Science 245 (1989) 845–847.
[10] (a) S. Lan, M. Veishe, M. Zhang, Biosens. Bioelectron. 20 (2005) 1697–1708;
(b) M. Veiseh, B.T. Wickes, D.G. Castner, M. Zhang, Biomaterials 25 (2004) 3315–3324.
[11] D.M. Kirschenbaum, Int. J.Pept. Protein Res. 4 (1972) 125–140.
[12] (a) C. Sieger, M. Biesalski, R. Haag, Chem. Eur. J. 10 (2004) 2831;
(b) Y. Kim, J. Koo, Ha, J. Appl. Surf. Sci. 249 (2005) 7–11;
(c) C. Pale-Grosdemange, E. Simon, K. Prime, G. Whitesides, J. Am. Chem. Soc. 113 (1991) 12–20;
(d) H. Sugimura, A. Hozumi, T. Kameyama, O. Takai, Surf. Interf. Anal. 34 (2002) 550–554;
(e) N. Faucheux, R. Schweiss, K. Lutzow, C. Werner, T. Groth, Biomaterials 25 (2004) 2721–2730.
[13] (a) M.D. Porter, T.B. Bright, D.L. Allara, C.E.D. Chidsey, J. Am. Chem. Soc. 109 (1987) 3559–3568;
(b) C.D. Bain, E.B. Troughton, Y.-T. Tao, J. Evall, G.M. Whitesides, R.G. Nuzzo, J. Am. Chem. Soc. 111 (1989) 321–335.
[14] Z. Mekhalif, J. Riga, J.J. Pireaux, J. Delhalle, Langmuir 13 (8) (1997) 2285–2290.
[15] I. Langmuir, J. Am. Chem. Soc. 40 (1918) 1361–1403.
[16] C.S. Chen, M. Mrksich, S. Huang, G.M. Whitesides, D.E. Ingber, Science 276 (1997) 1164–1167.
[17] (a) K.L. Prime, G.M. Whitesides, J. Am. Chem. Soc. 115 (1993) 10714–10721;
(b) M. Mrksich, G.B. Sigal, G.M. Whitesides, Langmuir 11 (1995) 4383–4385.
[18] M. Veiseh, B.T. Wickes, D.G. Castner, M. Zhang, Biomaterials 25 (2004) 3315–3324.
[19] K.M. Hansson, S. Tosatti, J. Isaksson, J. Wettero, M. Textor, T.L. Lindahl, P. Tengvall, Biomaterials 26 (2005) 861–872.
[20] S. Lan, M. Veiseh, M. Zhang, Biosens. Bioelectron. 20 (2005) 1697–1708.
[21] (a) P. Vermette, L. Meagher, Coll. Surf. B 28 (2003) 153–198, and references therein;
(b) M. Zheng, F. Davidson, X. Huang, J. Am. Chem. Soc. 125 (2003) 7790–7791;
(c) W. Inglis, G.H.W. Sanders, P.P. Williams, M.C. Davies, C.J. Roberts, S.J.B. Tendler, Langmuir 17 (2001) 7402–7405.
[22] (a) C. Bocca, O. Caputo, R. Cavalli, L. Gabriel, A. Miglietta, M.R. Gasco, Int. J. Pharm. 175 (1998) 185–193;
(b) R. Gref, M. Lück, P. Quellec, M. Marchand, E. Dellacherie, S. Harnisch, T. Blunk, R.H. Müller, Coll. Surf. B 18 (2000) 301–313.
[23] M.S. Kent, H. Yim, D.Y. Sasaki, Langmuir 20 (2004) 2819.
[24] F. MacRitchie, Adv. Protein Chem. 32 (1978) 283.
[25] J.H. Santos, N. Matsuda, Z.-M. Qi, T. Yoshida, A. Takatsu, K. Kato, Anal. Sci. 19 (2003) 199–204.